ADVANCED OPTICAL MATERIALS

www.advopticalmat.de

Vertical Cavity Biexciton Lasing in 2D Dodecylammonium Lead Iodide Perovskites

Edward P. Booker, Michael B. Price, Peter J. Budden, Haralds Abolins, Yago del Valle-Inclan Redondo, Lissa Eyre, Iyad Nasrallah, Richard T. Phillips, Richard H. Friend, Felix Deschler, and Neil C. Greenham**

Layered Ruddlesden-Popper-type (2D) metal-halide perovskites exhibit markedly increased exciton binding energies, exceeding 150 meV, compared to their 3D counterparts. Many-body physics, enabled by Coulomb interactions, plays a strong role and raises the biexciton binding energy to 50 meV. Here, photoluminescence at a range of temperatures and carrier concentrations in thin films of the layered perovskite material $(C_{12}H_{25}NH_3)_2PbI_4$ is reported. Biexcitons are directly observed up to a sample temperature of 225 K. An optical microcavity (comprising a distributed Bragg reflector and a metal mirror), with photonic resonances tuned near to the biexciton energy, is constructed. Optically-pumped biexciton lasing up to 125 K, with a threshold peak excitation density of 5.6×10^{18} cm^{-3}, is observed. The demonstration of biexciton lasing above liquid nitrogen temperatures is a crucial step for the application of layered perovskites in photonic applications.

Layered (2D) perovskites have been studied extensively for the last 30 years due to their potential optoelectronic applications (e.g., field-effect transistors,[1] light-emitting diodes (LEDs),[2] and solar cells,[3] mixed 2D–3D lasers[4]), wavelength tunability,[5] and the physics they exhibit as self-assembled alternating organic and inorganic sheets.[6,7]

In this work we study dodecylammonium lead iodide, $(C_{12}H_{25}NH_3)_2PbI_4$ (DA_2PbI_4), which consists of sheets of lead iodide octahedra separated by dodecylammonium ligands (**Figure 1**d–f). These ligands give high confinement in the inorganic layers, resulting in a large increase in the exciton binding energy,[8,9] which in this material has previously been determined to be 320 meV.[10]

E. P. Booker, Dr. M. B. Price, P. J. Budden, H. Abolins,
Dr. Y. del Valle-Inclan Redondo, L. Eyre, Dr. I. Nasrallah, Prof. R. T. Phillips, Prof. R. H. Friend, Dr. F. Deschler, Prof. N. C. Greenham
Cavendish Laboratory
J. J. Thomson Avenue, Cambridge CB3 0HE, UK
E-mail: fd297@cam.ac.uk; ncg11@cam.ac.uk

The ORCID identification number(s) for the author(s) of this article can be found under https://doi.org/10.1002/adom.201800616.

DOI: 10.1002/adom.201800616

We investigate the many-body interactions of excited species in the quantum wells formed in DA_2PbI_4, and identify biexciton formation with a binding energy of 50 meV. Biexcitons (stable four-particle states formed from the interaction of two excitons) have been well studied in quantum well structures[11,12] and are of interest for lasing applications due to their intrinsic potential for reducing self-absorption compared to conventional excitonic lasing schemes, for example in 3D or 2D–3D perovskites. As well as recent reports of wavelength-tunable amplified spontaneous emission (ASE) in 3D perovskites[13] and ASE in mixed 2D–3D perovskites[14] there have been previous reports of biexciton lasing at 16 K with high excitation densities.[15] Here we demonstrate biexciton lasing in cavities formed from this 2D perovskite above liquid nitrogen temperatures (125 K). We additionally observe emission from higher-lying energy states, which we attribute to the formation of more than one structural phase in the film.

Films of DA_2PbI_4 were spin-cast from solutions of dodecylammonium iodide and lead iodide onto glass as described previously.[16] The films are multicrystalline, and scanning electron microscope images suggest grain sizes in the range 1–10 µm (Figure S8, Supporting Information).

We examine the multiexciton properties of DA_2PbI_4 through a series of photon-intensity and temperature dependent photoluminescence (PL) measurements. We use the PL spectrum at low temperature for assignment of the species present. The film was excited at 3.10 eV with 200 fs laser pulses (1 kHz repetition rate), resulting in a peak carrier concentration of 9.6×10^{19} cm^{-3}. The time-integrated PL spectrum at 10 K is shown in Figure 1a. The Frenkel defects reported previously[16] are clearly seen around 2.0 eV (labelled **F**). There are four further emission peaks we have labelled **XX** (≈2.37 eV), **X** (≈2.42 eV—the main emission peak reported previously), **X′X′** (≈2.53 eV) and **X′** (≈2.58 eV). We identify **X** as the exciton emission of DA_2PbI_4 and **XX** as the biexciton resulting from two **X** excitons coupling together, as will be shown below. The lifetimes of all species aside from the Frenkel defects were shorter than the 3 ns instrument response time of our intensified charge-coupled device (iCCD). The contribution of each species to the overall PL was determined by modeling the PL data as five independent Gaussian peaks for

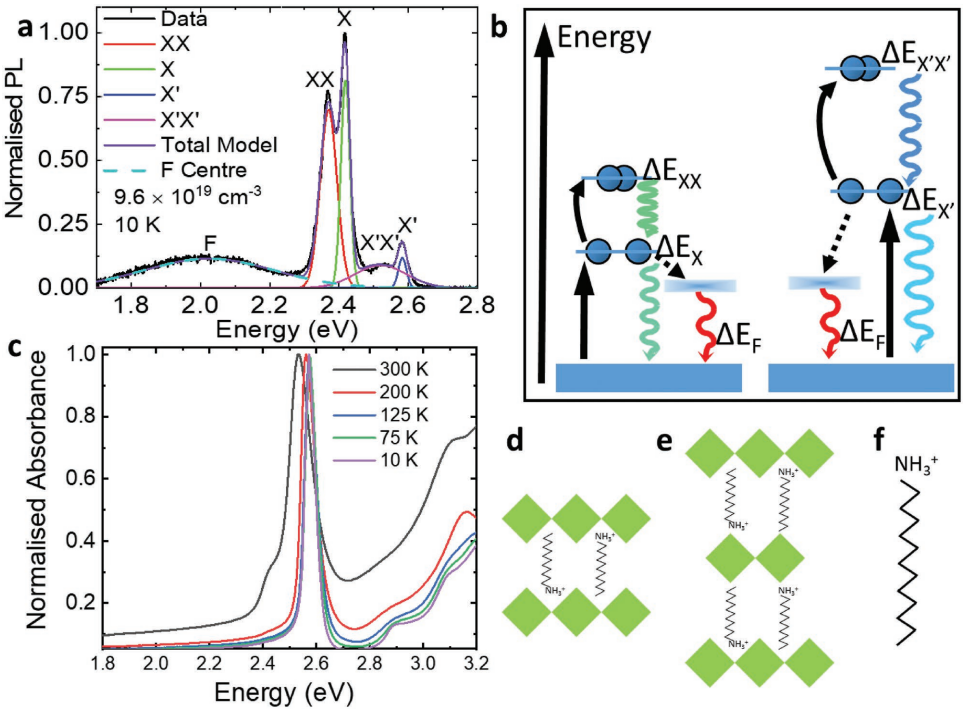

Figure 1. Steady-state photophysics of dodecylammonium lead iodide (DA_2PbI_4). a) Photoluminescence emission spectrum at 10 K (black trace) with gaussian fits to the various peaks overlaid. b) Proposed state diagram of the system. Excitation from the crystal ground state produces excitons in different grains either in **X** or **X′**; these can recombine or couple with similar excitons to form biexcitons, either **XX** or **X′X′** respectively. Frenkel defects (**F**) allow a terminal loss pathway out of the exciton manifold. c) Temperature-dependent absorption spectra for films on glass. Schematics of d) *$P_1$21/a* DA_2PbI_4 and e) *Pbca* DA_2PbI_4 as described by Booker et al.,[16] the low- and high-temperature phases respectively. f) Illustration of the dodecylammonium cation.

the identified states, and the associated uncertainty in the emission is taken from the error in the fit.

While the higher-energy peaks **X′** and **X′X′** have been observed in some previous studies,[16,17] their physical origins have yet to be commented on. The simplest explanation is that there are two coexisting phases of DA_2PbI_4 in a mechanical mixture with different exciton energies. Emission from light-hole excitons[18] or split-off bands might also be possible, as seen in 3D perovskites,[19] however, we do not see the excitation density dependence in the ratio of emission from **X** and **X′** that would be expected (**Figure 2**c inset). Spatially resolved photoluminescence microscopy measurements show distinct regions with dimensions exceeding 1 µm and single photoluminescence peaks centred at 2.4 and 2.5 eV (Figure S4, Supporting Information). This suggests that **X′** is due to a higher-energy phase in mechanical mixture with the phase responsible for **X**. Further evidence of separate **X** and **X′** phases is given by thin film XRD measurements (Figure S6, Supporting Information) which demonstrate that the films can be characterised by a mixture of *Pbca* and *$P_1$21/a* phases of DA_2PbI_4. Lattice parameters for these phases are given in Table S1 in the Supporting Information. Previously these phases have not been seen present in the same film.[16,20] Other explanations, such as charged defects or phonon replicas are not consistent with the peak being so far blue-shifted from the main emissive species. It should be noted that we do not observe the lower-energy peaks attributed to surface-bound excitons as seen by Chong et al.[21]; we only see the Frenkel defect emission reported previously.[16] An absence of additional defect states would explain the improved photophysical properties observed in this study, compared to some others.[21]

Figure 1b is a proposed state diagram based on these measurements: states **X** and **X′** are photoexcited with the 3.1 eV pump laser and may decay radiatively to the ground state. **X** may couple with **X** to form **XX** which may then decay radiatively back to **X**. A similar set of processes applies for **X′** and **X′X′**. The Frenkel defects provide terminal loss pathways, trapping charges and leading to broadband red emission.

Figure 2a inset shows the room-temperature emission at high excitation densities, which consists of two peaks, **X** and **X′**. Figure 2a shows the photoluminescence as the temperature is lowered at constant pump intensity. Both **X** and **X′** split into two peaks separated by ≈50 meV. This behaviour is also seen as the pump intensity is increased at constant temperature (Figure 2b).

The biexciton and the Frenkel defect appear to interact (Figure 2b). When the biexciton population grows, the Frenkel defect makes a smaller contribution relative to the total emission (Figure S2, Supporting Information). The ratio of integrated **XX** PL to integrated **F** PL increases with increasing pump intensity. This is consistent with a saturation of a finite number of F-centre sites as the carrier density is increased, concurrent with the onset of biexciton emission.

Figure 2c shows the intensity dependence of the integrated photoluminescence from **X** and **XX** and gives the power law dependence $PL \propto I_o^n$. Here I_o is the pump intensity and $n = 1.19 \pm 0.05$ for **XX**, 0.97 ± 0.05 for **X**, and 0.88 ± 0.05 for **X′**. The super-linear emission seen for **XX** is consistent with the behaviour expected for biexcitons.[22] Although Auger processes may compete with the formation of biexcitons, and may also compete with the

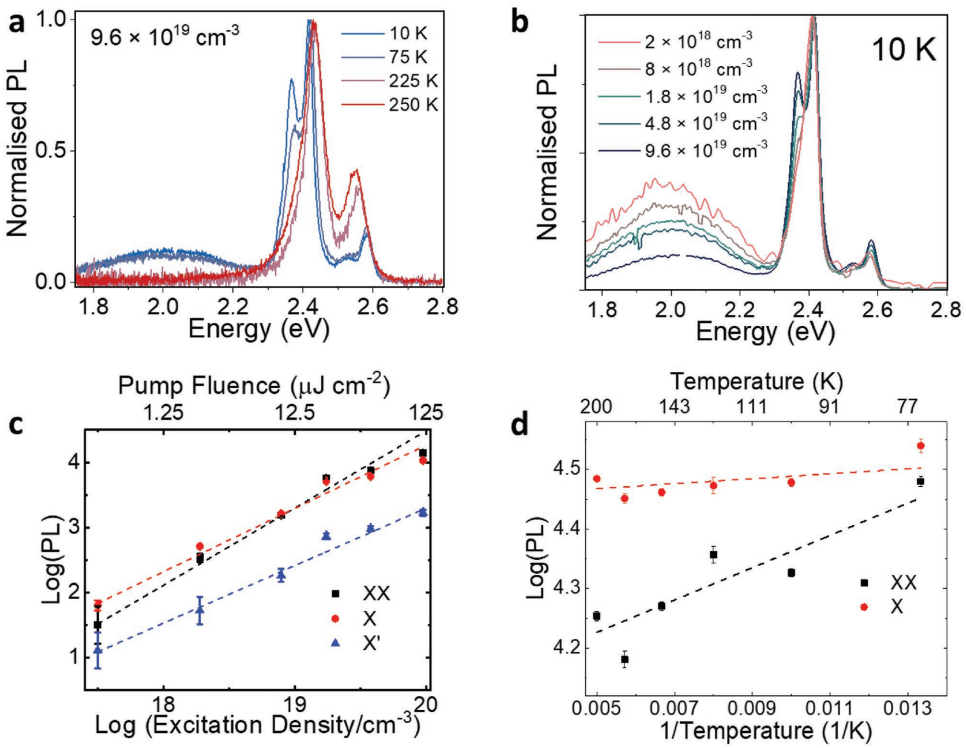

Figure 2. Temperature and power dependence of photoluminescence of DA_2PbI_4. Spectral features are those identified in Figure 1a. a) PL spectra at a carrier concentration of 9.6×10^{19} cm^{-3} from 10 to 250 K. The spectra are normalized to the emission peak of **X**. b) PL spectra at 10 K for the indicated carrier densities. The major emission features are the same as those in inset (a). c) The excitation density dependence of the photoluminescence of the **XX** peak **X** peak, and **X'** peak at 10 K. The gradients of these plots give power laws of 1.19 ± 0.05, 0.97 ± 0.05, and 0.88 ± 0.05 respectively. d) Arrhenius plot of photoluminescence yields of **XX** and **X** which yield activation energies of 2.3 ± 0.4 and 0.3 ± 0.2 meV respectively.

radiative emission from biexcitons, the fact that we see significant biexciton emission suggests that these non-radiative emission channels do not dominate. **X′X′** displays a similar energy offset from **X′** as **XX** from **X**, suggesting it may be a biexciton of **X′**.

The biexciton binding energy is defined as the difference in energy between two free excitons and the biexciton state, $\Delta_{XX} = 2E_X - E_{XX}$. When the biexciton decays radiatively it is assumed to produce an exciton and a photon, of energies $\hbar\omega_X$ and $\hbar\omega_{XX}$ respectively. Together these assumptions give a relationship for the biexciton binding energy:

$$\Delta_{XX} = \hbar\omega_X - \hbar\omega_{XX} \quad (1)$$

This establishes a biexciton binding energy of (50 ± 5) meV from our data, which is consistent with the biexciton binding energy range suggested by Thouin et al (40–57 meV)[17] in similar 2D perovskites. The regular exciton binding energy is estimated as Δ_X = (322 ± 3) meV, the difference between the onset of band absorption and the excitonic absorption peak. We calculate the ratio Δ_{XX}/Δ_X (the Haynes ratio)[23,24] as 0.17. This is in the range covered by other 2D quantum well systems exhibiting biexciton emission, such as WSe_2 ($\Delta_{XX}/\Delta_X = 0.14$)[22] or GaAs/AlGaAs quantum wells($\Delta_{XX}/\Delta_X \approx 0.2$),[24] as well as theoretical calculations.[25] Together with the intensity dependence, this confirms that **XX** is a biexciton. Figure 2d shows an Arrhenius plot of the intensities of **XX** and **X**; the activation energies obtained are 2.3 ± 0.43 and 0.3 ± 0.2 meV respectively.

The observation of strong biexcitonic emission poses questions for future devices made from this material. Does the biexciton represent a useful emission pathway for optoelectronic devices, or is it simply another loss pathway that hinders normal excitonic emission? As the films under investigation were ≈25 nm thick it is unsurprising that we do not see ASE in the photoluminescence spectra, agreeing with Chong et al.[21] However, the comparatively sharp line widths in this material stimulate further investigation of biexcitonic lasing in DA_2PbI_4, in addition to motivation from previous reports of lasing in a similar 2D perovskite.[15]

We constructed an optical cavity in the form of a vertical-cavity surface-emitting laser (VCSEL).[26,27] The cavity was constructed from a distributed Bragg reflector—DBR—(Edmund Optics 45° AOI cold mirror with 50% reflectance at 400 nm), a 25 nm active layer of DA_2PbI_4 as processed above, a spacer layer of 150 nm poly(methylmethacrylate) (PMMA), and then a 200 nm evaporated silver layer (**Figure 3**a). The cavities exhibit mode spacings of ≈50 THz which can be seen in cavity reflectance measurements (Figure S1d, Supporting Information), giving a large effective cavity length of ≈1.8 μm due to the modes penetrating the DBR. The cavity was cooled to temperatures ranging from 75 to 195 K and optically pumped with 3.1 eV, 200 fs laser pulses.

Figure 3c shows the emission spectra for a cavity at 75 K under a range of excitation densities. At high excitation densities, the spectra show a narrow emission feature associated with a cavity mode at 2.285 eV, which we assign to lasing from

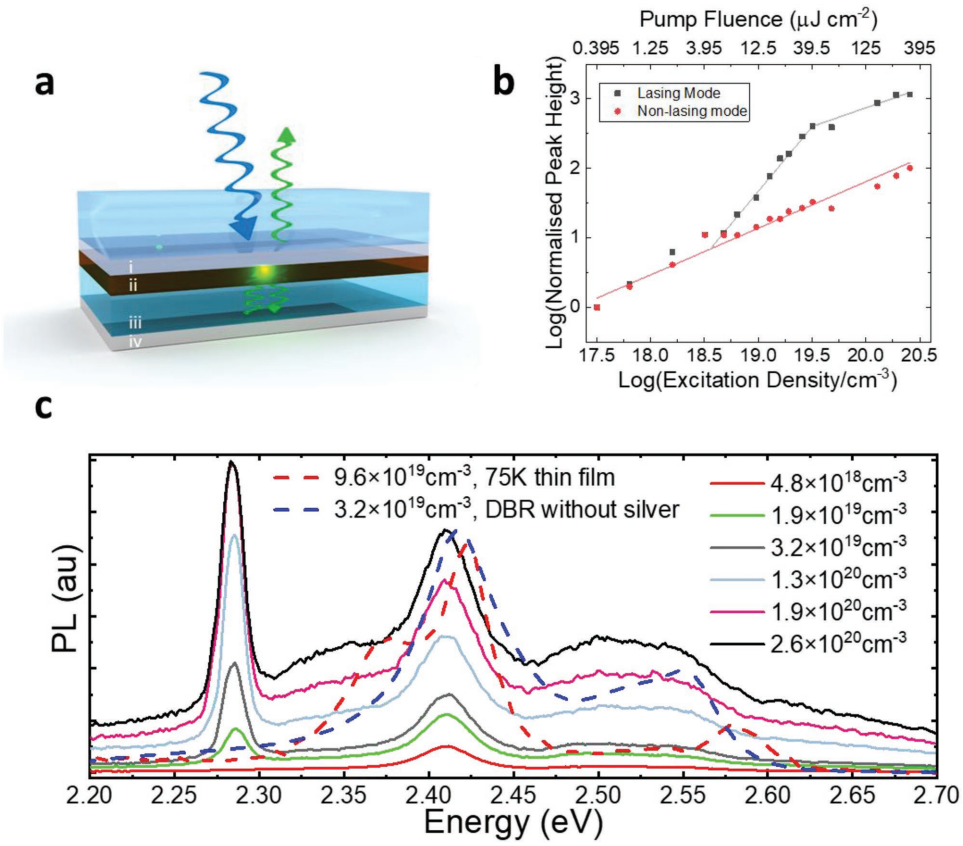

Figure 3. Demonstration of lasing from DA_2PbI_4 cavity. a) Schematic diagram of cavity architecture with approximate thicknesses of layers. (i) Distributed Bragg reflector (DBR) with (ii) 25 nm of spin-coated DA_2PbI_4, coated with (iii) ≈150 nm of PMMA with a (iv) 200 nm evaporated silver mirror on top. b) Excitation density dependence of the cavity emission at 2.28 and 2.41 eV. Lines of best fit are plotted. Emission intensities for each feature are normalized to the respective intensity at the lowest excitation density. c) Photoluminescence spectrum of cavity at different optical pump powers, PL of thin film of DA_2PbI_4 spun on glass, and PL response of the film on the DBR without the silver mirror on top. Measurements were taken with a series of excitation densities that were not monotonically increasing, in order to rule out significant degradation over the 4 h duration of the experiment.

the **XX** biexciton. This peak narrows with increasing excitation intensity (Figure S7, Supporting Information), as expected for lasing. Figure 3b compares the peak PL intensity of the **XX** cavity emission with emission from the non-amplifying cavity modes. The power law dependence ($\mathrm{PL} \propto I_o^n$) of the **XX** peak gives an exponent, *n*, that goes from 0.67 ± 0.02 before the kink (at ≈5.6×10^{18} carriers cm^{-3}) to 1.86 ± 0.04 after the kink, and then plateaus with a power law of 0.54 ± 0.04. This is in agreement with previous reports of biexciton lasing,[27,28] and shows the characteristic "s-like curve" expected for lasing.

Lasing occurs from the low-energy tail of the biexciton emission spectrum. Self-absorption losses will be minimised in this region. While the PL spectrum for films on glass (Figure 2) does not have significant overlap with the lasing cavity mode, there is a red-shift (roughly 25 meV) and broadening in the PL when films are deposited on the DBR (Figure 3c). This gives sufficient oscillator strength at the energy of the cavity mode for lasing to occur. The emission wavelength can be changed slightly by varying the cavity length (see Figure S1 (Supporting Information) for data on a second cavity). Lasing can be obtained at temperatures up to 125 K; Figure S3 (Supporting Information) shows similar threshold behaviour at 125 K as that observed at 75 K. Further optimisation of cavity mode energy and quality factor may allow further increases in operating temperature and reductions in threshold.

We show that for our fabrication conditions a layer of PMMA does not affect the low-energy emission from the exciton or the biexciton apart from introducing a small red shift of ≈5 meV (Figure S5, Supporting Information). This difference from Chong et al.[21] is likely due to the slightly different structures and annealing conditions used in this work.

The presence of biexcitons in DA_2PbI_4 at intermediate temperatures (up to 225 K) is firmly established in this work from measurements of the neat film. The very high biexciton binding energy, which is almost double the thermal energy at room temperature, suggests that room temperature populations of biexcitons may exist. Room temperature biexciton populations have previously been reported by Thouin et al.[17] in a slightly different material using a different experimental technique. We observed biexciton lasing at excitation densities of 5.6×10^{18} cm^{-3} at 75 K and 10^{19} cm^{-3} at 125 K. This, coupled with the appearance of biexciton emission in a cavity at higher temperatures, demonstrates the potential for high-temperature biexciton lasing. With improved materials processing and cavity construction this paves the way to room-temperature laser devices in this materials system.

Experimental Section

Film Preparation: DA_2PbI_4 films were spin-cast at 2000 rpm from a 1:2.5 molar ratio solution of lead iodide and dodecylammonium iodide at 20 mg mL^{-1}. Thickness was determined by ellipsometry of films spun on silicon. PMMA layers were prepared spun at 2000 rpm on top of spin-coated DA_2PbI_4 films from a solution of 7 mg mL^{-1} in chlorobenzene.

Intensified Charge-Coupled Device (iCCD) Cryostat Measurements: A portion of the output of a Ti:Sapphire amplifier system (Spectra-Physics Solstice) operating at 1 kHz was frequency-doubled using a β-barium borate crystal to generate excitation pulses at 400 nm, with a duration of ≈200 fs. The beam was focussed to a spot size of 400 µm onto the sample in an inert atmosphere in a cryostat (CF-V, Oxford Instruments), cooled with liquid helium to temperatures from 10 to 295 K. Emitted light was collected and focussed onto the slits of a Shamrock 303i Andor spectrometer coupled to an integrated charge-coupled device (iCCD - iStar DH740 Andor).

Reflectance Measurements: Reflectivity spectrum at room temperature was taken with a 0.5 meV resolution spectrometer (10 s integration time), through a 0.25 NA microscope objective using a silver mirror as a reflectivity reference.

Supporting Information

Supporting Information is available from the Wiley Online Library or from the author. The data underlying this publication are available at https://doi.org/10.17863/CAM.25934.

Acknowledgements

E.P.B. and M.B.P. contributed equally to this work. This work was supported by the EPSRC [Grant numbers EP/P02484X/1, EP/M005143/1, and EP/L01551X/1 (Centre for Doctoral Training in Photovoltaics)]. F.D. acknowledges an Advanced Fellowship from the Winton Programme for the Physics of Sustainability.

Conflict of Interest

The authors declare no conflict of interest.

Keywords

biexcitons, lasing, perovskites, photoluminescence

Received: May 9, 2018
Revised: July 18, 2018
Published online:

[1] C. R. Kagan, D. B. Mitzi, C. D. Dimitrakopoulos, *Science* **1999**, *286*, 945.
[2] M. Yuan, L. N. Quan, R. Comin, G. Walters, R. Sabatini, O. Voznyy, S. Hoogland, Y. Zhao, E. M. Beauregard, P. Kanjanaboos, Z. Lu, D. H. Kim, E. H. Sargent, *Nat. Nanotechnol.* **2016**, *11*, 872.
[3] D. H. Cao, C. C. Stoumpos, O. K. Farha, J. T. Hupp, M. G. Kanatzidis, *J. Am. Chem. Soc.* **2015**, *137*, 7843.
[4] H. Zhang, Q. Liao, Y. Wu, Z. Zhang, Q. Gao, P. Liu, M. Li, J. Yao, H. Fu, *Adv. Mater.* **2018**, *30*, 1.
[5] P. Lova, D. Cortecchia, H. N. Swaha Krishnamoorthy, P. Giusto, C. Bastianini, A. Bruno, D. Comoretto, C. Soci, H. N. S. Krishnamoorthy, P. Giusto, C. Bastianini, A. Bruno, D. Comoretto, C. Soci, *ACS Photonics* **2018**, *5*, 867.
[6] K. Tanaka, F. Sano, T. Takahashi, K. E. Takashi Kondo, R. Ito, *Solid State Commun.* **2002**, *122*, 249.
[7] S. Neutzner, F. Thouin, D. Cortecchia, A. Petrozza, C. Silva, A. R. S. Kandada, *Phys. Rev. Mater.* **2018**, *2*, 064605.
[8] T. Ishihara, J. Takahashi, T. Goto, *Solid State Commun.* **1989**, *69*, 933.
[9] X. Hong, T. Ishihara, a. V. Nurmikko, *Phys. Rev. B* **1992**, *45*, 6961.
[10] T. Ishihara, J. Takahashi, T. Goto, *Phys. Rev. B* **1990**, *42*, 11099.
[11] R. T. Phillips, D. J. Lovering, G. J. Denton, G. W. Smith, *Phys. Rev. B* **1992**, *45*, 4308.
[12] G. J. Denton, R. T. Phillips, G. W. Smith, *Appl. Phys. Lett.* **1995**, *67*, 238.
[13] G. Xing, N. Mathews, S. S. Lim, N. Yantara, X. Liu, D. Sabba, M. Grätzel, S. Mhaisalkar, T. C. Sum, *Nat. Mater.* **2014**, *13*, 476.
[14] M. Li, Q. Gao, P. Liu, Q. Liao, H. Zhang, J. Yao, W. Hu, Y. Wu, H. Fu, *Adv. Funct. Mater.* **2018**, *28*, 1707006.
[15] T. Kondo, T. Azuma, T. Yuasa, R. Ito, *Solid State Commun.* **1998**, *105*, 253.
[16] E. P. Booker, T. H. Thomas, C. Quarti, M. R. Stanton, C. D. Dashwood, A. J. Gillett, J. M. Richter, A. J. Pearson, N. J. L. K. Davis, H. Sirringhaus, M. B. Price, N. C. Greenham, D. Beljonne, S. E. Dutton, F. Deschler, *J. Am. Chem. Soc.* **2017**, *139*, 18632.
[17] F. Thouin, S. Neutzner, D. Cortecchia, V. A. Dragomir, C. Soci, T. Salim, Y. M. Lam, R. Leonelli, A. Petrozza, A. R. S. Kandada, C. Silva, *Phys. Rev. Mater.* **2017**, *034001*, 1.
[18] S. Ithurria, B. Dubertret, *J. Am. Chem. Soc.* **2008**, *130*, 16504.
[19] J. Even, L. Pedesseau, J. M. Jancu, C. Katan, *J. Phys. Chem. Lett.* **2013**, *4*, 2999.
[20] D. G. Billing, A. Lemmerer, *New J. Chem.* **2008**, *32*, 1736.
[21] W. K. Chong, K. Thirumal, D. Giovanni, T. W. Goh, X. Liu, N. Mathews, S. Mhaisalkar, T. C. Sum, *Phys. Chem. Chem. Phys.* **2016**, *18*, 14701.
[22] Y. You, X.-X. Zhang, T. C. Berkelbach, M. S. Hybertsen, D. R. Reichman, T. F. Heinz, *Nat. Phys.* **2015**, *11*, 477.
[23] J. R. Haynes, *Phys. Rev.* **1960**, *4*, 361.
[24] D. Birkedal, J. Singh, V. G. Lyssenko, J. Erland, J. M. Hvam, *Phys. Rev. Lett.* **1996**, *76*, 672.
[25] J. Singh, D. Birkedal, V. Lyssenko, J. Hvam, *Phys. Rev. B: Condens. Matter Mater. Phys.* **1996**, *53*, 15909.
[26] F. Deschler, M. Price, S. Pathak, L. E. Klintberg, D. D. Jarausch, R. Higler, S. Hüttner, T. Leijtens, S. D. Stranks, H. J. Snaith, M. Atatüre, R. T. Phillips, R. H. Friend, *J. Phys. Chem. Lett.* **2014**, *5*, 1421.
[27] Y. Harada, H. Kondo, S. Hashimoto, *J. Appl. Phys.* **2005**, *98*, 1.
[28] J. Q. Grim, S. Christodoulou, F. Di Stasio, R. Krahne, R. Cingolani, L. Manna, I. Moreels, *Nat. Nanotechnol.* **2014**, *9*, 891.